THE JOURNAL OF BIOLOGICAL CHEMISTRY VOL. 289, NO. 11, pp. 7702–7717, March 14, 2014

Naphthoquinone-mediated Inhibition of Lysine Acetyltransferase KAT3B/p300, Basis for Non-toxic Inhibitor Synthesis*

Received for publication, May 18, 2013, and in revised form, January 20, 2014 Published, JBC Papers in Press, January 27, 2014, DOI 10.1074/jbc.M113.486522

Mohankrishna Dalvoy Vasudevarao[‡1], Pushpak Mizar[‡1], Sujata Kumari[‡1], Somnath Mandal[‡], Soumik Siddhanta[§], Mahadeva Swamy MM[‡], Stephanie Kaypee[‡], Ravindra Kodihalli C[‡], Amrita Banerjee[¶], Chandrabhas Naryana[§], Dipak Dasgupta[¶], and Tapas K. Kundu[‡2]

From the [‡]Transcription and Disease Laboratory and the [§]Light Scattering Laboratory, Jawaharlal Nehru Centre for Advanced Scientific Research, Jakkur, Bangalore-560064, Karnataka, India and the [¶]Biophysics and Structural Genomics Division, Saha Institute of Nuclear Physics, Kolkata-700064, West Bengal, India

Background: 1,4-Naphthoquinone analogs, such as plumbagin, are toxic compounds due to their redox cycling and thiol-reactive properties.
Results: The p300 inhibitor PTK1, a plumbagin derivative with greatly reduced toxicity, was synthesized and characterized.
Conclusion: PTK1 is a reversible, non-competitive inhibitor of p300 KAT activity with reduced toxicity.
Significance: These studies provide insight into naphthoquinone-mediated KAT inhibition and describe the synthesis of a therapeutically important, non-toxic inhibitor.

Hydroxynaphthoquinone-based inhibitors of the lysine acetyltransferase KAT3B (p300), such as plumbagin, are relatively toxic. Here, we report that free thiol reactivity and redox cycling properties greatly contribute to the toxicity of plumbagin. A reactive 3rd position in the naphthoquinone derivatives is essential for thiol reactivity and enhances redox cycling. Using this clue, we synthesized PTK1, harboring a methyl substitution at the 3rd position of plumbagin. This molecule loses its thiol reactivity completely and its redox cycling ability to a lesser extent. Mechanistically, non-competitive, reversible binding of the inhibitor to the lysine acetyltransferase (KAT) domain of p300 is largely responsible for the acetyltransferase inhibition. Remarkably, the modified inhibitor PTK1 was a nearly non-toxic inhibitor of p300. The present report elucidates the mechanism of acetyltransferase activity inhibition by 1,4-naphthoquinones, which involves redox cycling and nucleophilic adduct formation, and it suggests possible routes of synthesis of the non-toxic inhibitor.

Over the past decade, several small molecule modulators of chromatin-modifying enzymes have been discovered (1, 2). These molecules include specific and nonspecific inhibitors of histone deacetylases, histone acetyltransferases (now known as lysine acetyltransferases or KATs),[3] histone methyltransferases, and specific activators of the lysine acetyltransferases 3B/3A (p300/CBP). 1,4-Naphthoquinone derivatives are naturally occurring compounds that are present in the *Plumbago* and *Diospyros* plant genera and have a variety of biological activities (3). Our laboratory previously reported that one of the 1,4-naphthoquinones, plumbagin, is a potent inhibitor of the KAT p300. Plumbagin specifically inhibits p300-mediated p53 acetylation but not the p53 acetylation by the lysine acetyltransferase KAT2B (p300/CBP-associated factor) (4). This study described for the first time that a structural entity (a hydroxyl group at the 5th position of plumbagin) is required for the inhibition of acetyltransferase activity. However, naphthoquinone derivatives are relatively toxic molecules, and their efficacy and utility *in vivo* has been limited due to this characteristic (5–8). The aim of the present study is to understand the mechanism of KAT inhibition as well as the chemical entity responsible for its cytotoxicity and, thus, to synthesize a non-toxic KAT inhibitor.

Among the different small molecule KAT inhibitors known to date, Lys-CoA was the first to be discovered as a p300 acetyltransferase-specific inhibitor (9). The catalytic mechanisms of the enzyme have been investigated from the co-crystal structural analysis of the p300 KAT domain and Lys-CoA (10). Lys-CoA interacts extensively with the acetyltransferase domain, particularly in the hydrophobic tunnel. Lys-CoA-mediated inhibition supports a Theorell-Chance model rather than a standard ordered binding, ternary complex, or ping-pong mechanism. Based on the residues that Lys-CoA binds within the hydrophobic tunnel, a new enzyme-inhibitory scaffold, C646, has been synthesized by the same group (11). Over the years, we have discovered a few naturally occurring, small molecule KAT inhibitors (4, 12–16). Our investigations have

* This work was supported by the Department of Biotechnology, Government of India (Program Support for Chromatin and Disease, Sanction Code BT/01/CEIB/10/III/01/dt-30.09.2011) and the Jawaharlal Nehru Centre for Advanced Scientific Research.
[1] These authors contributed equally to this work.
[2] Supported by a Sir J. C. Bose Fellowship (Department of Science and Technology, Government of India). To whom correspondence should be addressed. Tel.: 80-22082840; 80-22082841; Fax: 91-80-22082766; E-mail: tapas@jncasr.ac.in.
[3] The abbreviations used are: KAT, lysine acetyltransferase; HAT, histone acetyltransferase; DTNB, 5,5′-dithiobis(nitrobenzoic acid); PTK1, 5-hydroxy-2,3-dimethylnaphthalene-1,4-dione; CBP, CREB-binding protein; CREB, cAMP-response element-binding protein; MTT, 3-(4,5-dimethylthiazol-2-yl)-2,5-diphenyltetrazolium bromide; ROS, reactive oxygen species; NAC, *N*-acetyl cysteine; SERS, surface-enhanced Raman spectroscopy; H3K9, histone H3 Lys-9.

revealed that there are pockets in the p300 acetyltransferase KAT domain, other than the hydrophobic tunnel, where these small molecules may bind and cause enzyme inhibition (4, 17). These p300 inhibitors, such as garcinol, plumbagin, and the p300-specific garcinol derivative LTK14, have at least one binding site within the KAT domain (17). A docking analysis with plumbagin has shown that binding may not occur in the hydrophobic tunnel of the KAT domain, suggesting that other binding pockets might exist (4). Although the mechanisms of action for these small molecule inhibitors have been investigated in terms of enzyme binding and kinetics, the chemical nature of these small molecules has received much less attention. Notably, most KAT inhibitors consist of hydroxyl groups, leading to speculation that the -OH groups could facilitate enzyme-small molecule interactions and thereby KAT inhibition (4). In this respect, we have previously reported that the activity of plumbagin can be ascribed to the hydrogen bonding between the hydroxyl group and Lys-1358 in the KAT domain (4). However, plumbagin is known to react with free -SH (thiol) groups available in the intracellular milieu, including glutathione, and is also involved in redox cycling. These chemical properties of 1,4-naphthoquinones, such as plumbagin, may be the cause of their cytotoxicity and may influence their KAT-inhibitory activity. The toxicity also hampers their utility (5–8). Therefore, we are interested in investigating the role of the chemical nature of plumbagin and other related 1,4-naphthoquinone analogs in KAT inhibition and cytotoxicity with the ultimate goal of synthesizing a non-toxic, reversible inhibitor.

Our results suggest that the major mechanism of plumbagin-mediated KAT inhibition is through irreversible protein interactions. However, the cytotoxicity of plumbagin analogs is due to their ability to generate reactive oxygen species as well as their reactivity to thiols. The structure-function relationships of these 1,4-naphthaquinones lead us to the conclusion that the structural moieties responsible for KAT inhibition and those responsible for toxicity do not overlap and can be delineated. Based on these observations, we have synthesized a new molecule that does not have free thiol reactivity and has less redox cycling potential but retains KAT inhibitory activity. Thus, this molecule could potently reduce histone acetylation in cell-based assays with greatly decreased toxicity.

EXPERIMENTAL PROCEDURES

Cell Culture, Treatments, and Immunoblotting—SHSY-5Y (human neuroblastoma) and HEK293 (human embryonic kidney) cells were cultured in Dulbecco's modified Eagle's medium (DMEM) with 10% fetal bovine serum (FBS) at 37 °C and 5% CO_2 in an incubator. HeLa S3 cells were cultured in F-12K (Invitrogen) medium supplemented with 10% FBS. Cells (3×10^6 cells/60-mm dish) were seeded and then treated 12 h later with plumbagin and other compounds at the desired concentrations for 6 h. In the case of *N*-acetyl cysteine (NAC) treatment, the cells were pretreated with 2 mM NAC for 2 h prior to the addition of plumbagin. After collecting cells at the indicated time points, cell lysates were prepared using Laemmli sample buffer (60 mM Tris-Cl, pH 6.8, 2% SDS, 10% glycerol, 5% β-mercaptoethanol, and 0.01% bromphenol blue). The proteins were separated on acrylamide gels, and immunoblotting analysis was performed. Briefly, the proteins were resolved on 12% SDS-polyacrylamide gels and transferred to nitrocellulose membranes using a semidry transfer apparatus (Bio-Rad). Membranes containing the transferred proteins were blocked using 5% skim milk solution. The membranes were probed using polyclonal antibodies against histone H3K9 acetylation (Abcam, ab16635), H2AXγ (Abcam, 11174), and H3 (laboratory reagent) for 3 h at 4 °C. These membranes were incubated with a horseradish peroxidase-conjugated anti-IgG antibody (Bangalore Genei). After the addition of an HRP substrate (PICO West, Thermo Scientific) to the membrane, luminescent bands were captured using x-ray films.

Cell Viability Assay—For quantitation of cell viability, we performed a 3-(4,5-dimethylthiozol-2-yl)-2,5-diphenyltetrazolium bromide (MTT) assay. SHSY-5Y cells were seeded in 96-well plates (5000 cells/well). After 12 h, naphthoquinone derivatives were resuspended in the culture medium and added to the wells at the desired concentrations. After 24 h, the compound-containing medium was removed, and equal volumes of fresh medium were added to each well along with 20 μl of MTT (Sigma; 5 mg/ml in PBS). As expected, MTT was reduced to purple-colored formazan only in viable cells. After incubation for 4 h, DMEM was removed by syringe, and the formazan crystals were redissolved in 200 μl of DMSO. The plate was incubated at 37 °C for 5 min. The color was quantified with an ELISA plate reader (Versa Max ELISA plate reader, Molecular Devices, 595-nm wavelength).

Detection and Measurement of ROS—HEK293 and HeLa cells were grown in their respective media to 75% confluence. For fluorescence-based images, cells were grown on coverslips coated with poly-L-lysine. Cells were washed with PBS and treated with 5 μM CM-H2DCFDA (Invitrogen) for 20 min at 37 °C under 5% CO_2. The cells were then treated with different concentrations of compounds for the indicated times. Later, the cells were trypsinized and resuspended in PBS, and the fluorescence intensity was measured by flow cytometry. The sample was excited at 485 nm, and fluorescence was measured at 530 nm. For imaging, coverslips containing cells were washed with PBS and were mounted onto a glass slide using 70% glycerol as a mountant. Images were captured using a Zeiss Axioskop 2 Plus fluorescence microscope.

Lysine Acetyltransferase Assay (Filter-binding Assay)—Lysine acetyltransferase assays were performed as described previously (9). In brief, 800 ng of highly purified HeLa core histones was incubated in HAT assay buffer at 30 °C for 10 min with baculovirus-expressed recombinant p300 or CBP in the presence or absence of select compounds. This procedure was followed by the addition of 1.0 μl of 3.6 Ci/mM [^{3}H]acetyl-CoA (PerkinElmer Life Sciences). This mixture was further incubated for 10 min. The reaction mixture was then kept on ice for 5 min to stop the reaction, spotted onto P81 (Whatman) filter paper, and dried. Scintillation counts were recorded on a Wallac 1409 liquid scintillation counter. All assays were performed in replicates, and the average was plotted, with *error bars* indicating the S.D.

DTNB Assay and UV-visible Absorption/Emission Spectrometry—DTNB solution (3 mg/ml) was prepared in potassium phosphate buffer (100 mM, pH 6.8). NAC, DTT, and 1,4-naphtho-

quinone derivatives were dissolved in 100 mM DMSO. Initially, increasing concentrations of NAC and DTT (25–150 μM) were added to 100 μl of phosphate buffer. 1,4-Naphthoquinone derivatives were subsequently added to make a final concentration of 50 μM. An incubation time of 5 min at room temperature was followed by the addition of 100 μl of DTNB solution, maintaining the total reaction volume as 200 μl in all cases. The reaction was allowed to proceed for 5 min at room temperature, and the absorbance of the solution was analyzed at 412 nm using a Versa Max ELISA plate reader (Molecular Devices). For performing UV-visible absorption spectrometry, 1,4-naphthoquinone derivatives (1 mM in DMSO) were diluted in 1 ml of 100 mM potassium phosphate buffer (pH 6.8) or 100 mM HEPES buffer (pH 7.5) and were scanned for UV-visible absorption from 200 to 600 nM. Subsequently, NAC (1 mM in DMSO) was added, wherever necessary, to the buffer containing the derivatives, and scanning was repeated. The absorption spectrum was read using a spectrophotometer (U-2010, Hitachi). The same sets of solutions were also used for measuring the excitation wavelength and emission spectra using FluoroMax-3 (Horiba Jobin Yvon).

Kinetic Characterization—Lysine acetyltransferase assays were carried out with an ectopically expressed baculoviral construct encoding full-length p300, in the absence or presence of different concentrations of the inhibitor PTK1 (0, 15, 20, 25, 35, and 45 μM). The enzyme is known to catalyze a bisubstrate reaction comprising two substrates, namely core histone and [^{3}H]acetyl-CoA. Therefore, a kinetic analysis was performed on two different combinations. The enzyme activity was determined at increasing concentrations (1–8 μM) of [^{3}H]acetyl-CoA while keeping the concentration of core histones constant at 1.7 μM. In the second combination, the [^{3}H]acetyl-CoA concentration was kept constant at 1.6 μM while the core histone concentrations were varied from 5 to 70 nM. The reaction velocity was determined as a function of the incorporation of radioactivity and was expressed as counts/min (cpm). All of the experiments were conducted in triplicate, and the values were within 15% of the error range. The Michaelis-Menten plot was generated using the model, $y = V_{max} \times [S]/(K_m + [S])$. The K_i was determined by fitting to a straight line by the least square method in a Lineweaver-Burk plot using GraphPad prism version 5.0 software.

Reversibility Studies—The reversibility of the inhibitors was established by the time-dependent dilution and "drop dialysis" methods. For dialysis, the enzyme p300 was incubated with inhibitors for 30 min, and the mixture was dialyzed at 4 °C against 2× HAT assay buffer using 0.05-μm Millipore "V series membrane" to remove the inhibitors. The residual activity was assayed and compared with the predialysis activity. For time-dependent dilution-based experiments, full-length p300 was preincubated in 1× HAT assay buffer at pH 8.0 with either enzyme alone or with increasing concentrations (25–100 μM) of inhibitors with varying preincubation times (1–15 min). Aliquots of an appropriate volume were taken from each reaction mixture to make it final 1:25 dilution in every case. From each reaction mixture, the residual activity was measured as a percentage of the control and plotted against the preincubation time. Semilogarithmic plots were constructed, and the data were fit using the semilog line module of GraphPad prism version 5.0. The rate of inactivation was measured by fitting to the equation, $y = y$ intercept + slope × log(x), where x is logarithmic, y is linear, and the rate is equivalent to the slope equal to the apparent inactivation constant (k_{obs} per min) at each inhibitor concentration.

Dynamic Light Scattering—The measurements were performed on a Zetasizer Nano S particle analyzer (Malvern Instruments) with a helium-neon laser (632.8 nm) light source that utilizes 4-milliwatt power at the same wavelength. Scattered light from the samples was collected at an angle of 173°. The built-in software generates a correlation curve from the intensity autocorrelation function. The intensity-weighted mean hydrodynamic diameter, or Z_{av} diameter, of the sample was obtained from the cumulants analysis of the correlation curve. To study the effect of plumbagin, PTK1, and juglone on p300 oligomerization and compare their adduct-forming abilities, 5 μM p300 in 10 mM Tris-HCl at pH 7.5 containing 150 mM NaCl was treated with increasing concentrations (25–100 μM) of the three compounds, and the Z_{av} diameters of treated and untreated p300 were monitored by dynamic light scattering. Ten measurements (10 runs for each measurement) were recorded for each sample at 25 °C. Because the compounds are dissolved in DMSO, in control experiments, p300 was treated with an equal volume of DMSO without the compound(s), and the hydrodynamic parameters mentioned above were checked to confirm the absence of any alteration.

Surface-enhanced Raman Spectroscopy (SERS) Analysis—SERS spectra were recorded in a Raman system using 180° back-scattering geometry and a 632.8-nm helium-neon laser (model 30995, Research Electro Optics, Inc.) as a Raman excitation source (18, 19). The spectrometer consists of a monochromator (HORIBA JOBIN YVON, iHR 320) and a Peltier-cooled CCD (Andor iDus). A holographic 1800 grooves mm^{-1} grating was used along with the 200-μm spectrograph entrance slit setting, providing ~3 cm^{-1} resolution. For SERS studies of protein, a 60× infinity-corrected objective (Nikon Plan Apo; numerical aperture 0.9) was used. The laser power used at the sample was 5 milliwatts. Samples were prepared by concentrating the silver nanoparticles to 10 times, and a concentrated nanoparticle solution/analyte ratio of 4:1 was maintained. The typical accumulation time of 30 s was used. The SERS spectrum was smoothened using a standard five-point fast Fourier transform filtering technique, as shown in Fig. 9*D*. The silver solution was prepared as reported previously (20). Initially, 45 mg of $AgNO_3$ was dissolved in 250 ml of water, and the solution was brought to a boil. A solution of 1% sodium citrate (5 ml) was then added to the $AgNO_3$ solution under vigorous stirring, and boiling was continued for ~60 min. The plasmon absorption maximum was located at 420 nm.

Docking Studies—The crystal structure of p300 KAT domain was extracted from the Protein Data Bank using the code 3BIY. The structure of the inhibitor PTK1 was optimized using the GAUSSIAN 03 program (21). Docking analysis was performed with Autodock version 4.2 using a Lamarckian genetic algorithm. A 5-grid spacing of 0.375 was used, and docking was performed with a flexible ligand with 100 Genetic Algorithm runs, a population size of 300, 25 × 10^5 evaluations, and a max-

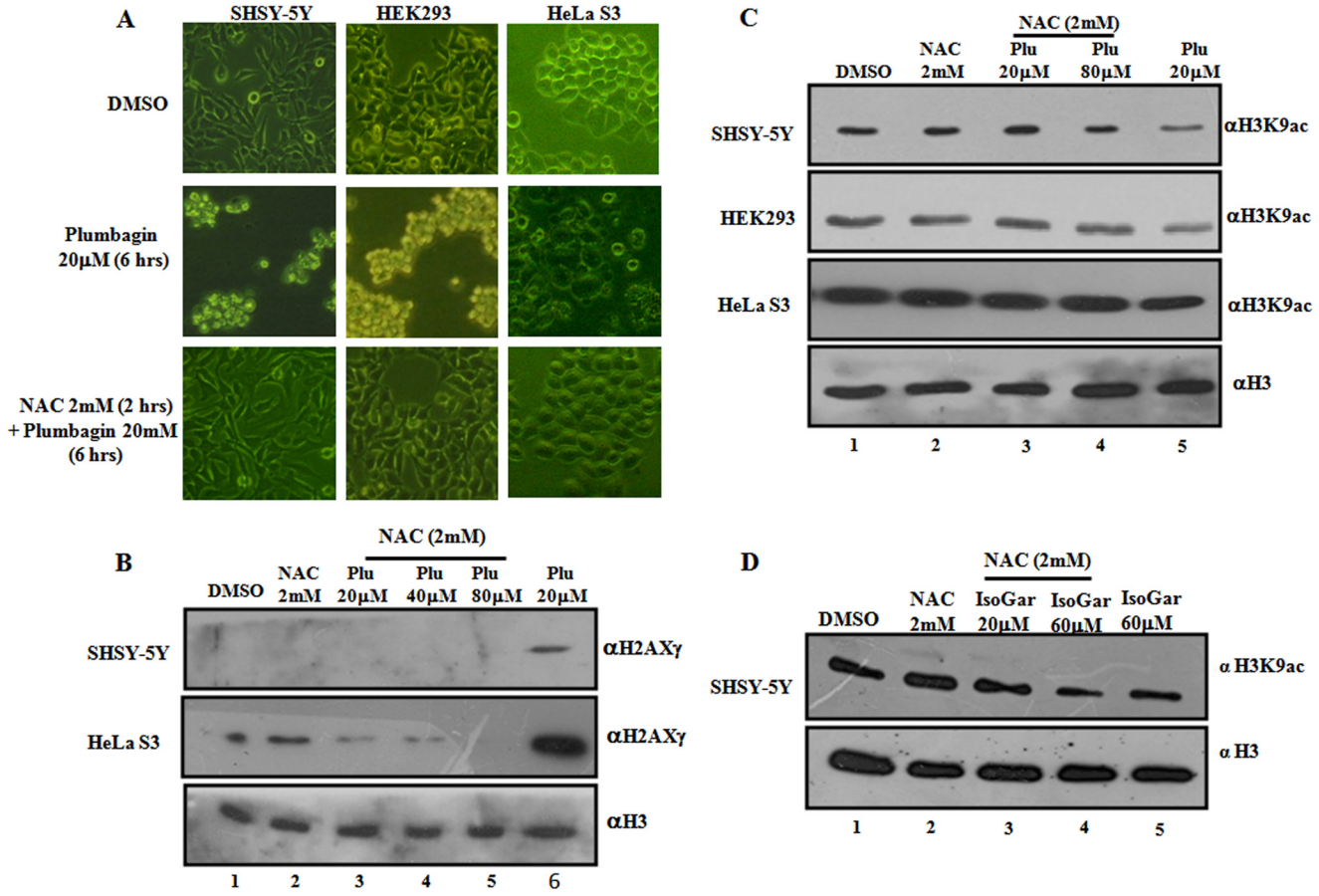

FIGURE 1. ***N*-Acetyl cysteine blocks plumbagin-mediated inhibition of histone acetylation and DNA damage in multiple mammalian cell lines.** *A*, images of SH-SY5Y, HEK293, and HeLa S3 cells, 6 h after treatment with DMSO, plumbagin, and plumbagin in the presence of NAC. *B*, immunoblotting (*IB*) analysis of H2AX phosphorylation (*H2AXγ*) after plumbagin (*Plu*) treatment in the presence or absence of NAC. *C*, immunoblotting analysis of histone H3K9 acetylation after plumbagin treatment in the presence or absence of NAC in the indicated cell lines; DMSO was used as solvent control, and immunoblotting with H3 antibodies was considered as loading control in *B* and *C*. *D*, immunoblotting analysis of histone H3K9 acetylation after isogarcinol (*IsoGar*) treatment in the presence or absence of NAC in the SH-SY5Y cell line; DMSO was used as solvent control, and immunoblotting with H3 antibodies was considered as loading control.

imum of 27,000 generations (22). The analysis of conformations was conducted based on clusters generated using MGL Autodock tools version 1.5.4. Figures were created using the PyMOL molecular graphics system (23).

Synthesis of 5-Hydroxy-2,3-dimethylnaphthalene-1,4-dione (PTK1)—PTK1 was synthesized as reported elsewhere (24). Plumbagin was isolated in our laboratory from *Plumbago rosea* as reported previously (4). PTK1 was synthesized by mixing plumbagin (1 mM), acetic acid (12 mM) as a radical source, and benzene (80 ml) as the solvent. The reaction mixture was cooled over dry ice and methanol until the solvent was frozen. The flask was degassed *in vacuo* for 15 min and filled with nitrogen. This degassing process was repeated three times. After adding lead tetra-acetate (3 mM), the flask was placed in an oil bath, and the mixture was refluxed under a nitrogen atmosphere for 24 h. Upon completion, the reaction was quenched with water to decompose the excess lead tetra-acetate. The organic layer was dried over anhydrous Na_2SO_4 and evaporated. The obtained crude product was purified by column chromatography using hexane/ethyl acetate (8.5:1.5).

^{1}H NMR and HRMS characterization of PTK1 were performed as described previously (15). The chemical structure was confirmed by following parameters: Orange Needles, yield 59%, 1H NMR (400 MHz, CDCl3) δ 2.17 (s, 6H, 2 CH3), 7.52–7.64 (m, 3H, Ar-3H), 12.16 (s, 1H, OH). HRMS (*m*/*z*): calculated for C12H10O3, 203.0663; found 203.0681.

Chemicals and Instruments—All of the chemicals were purchased from Sigma-Aldrich. Mass spectrometry was performed with a high resolution mass spectrometer (Agilent Technologies), and NMR spectra were obtained from a Bruker (400-MHz) NMR spectrometer.

RESULTS

N-Acetyl Cysteine Blocks Plumbagin-mediated KAT Inhibition as Well as Its Pleiotropic Effects in Vivo—Plumbagin is a known redox-cycling and free thiol-reactive molecule (25–27). Both of these properties influence its KAT-inhibitory properties in cells. Because there are earlier reports that are contradictory with respect to the role of ROS in histone acetylation (28–30), we investigated the potential effect of ROS generation in KAT-inhibitory activity and cytotoxicity. To do this, we treated the mammalian cell lines SH-SY5Y, HEK293, and HeLa S3 with plumbagin in the presence of the free radical scavenger NAC. As observed from the images of cells photographed after 6 h of treatment, NAC completely negated plumbagin-induced cell stress (Fig. 1*A*). Plumbagin induced DNA damage, presumably,

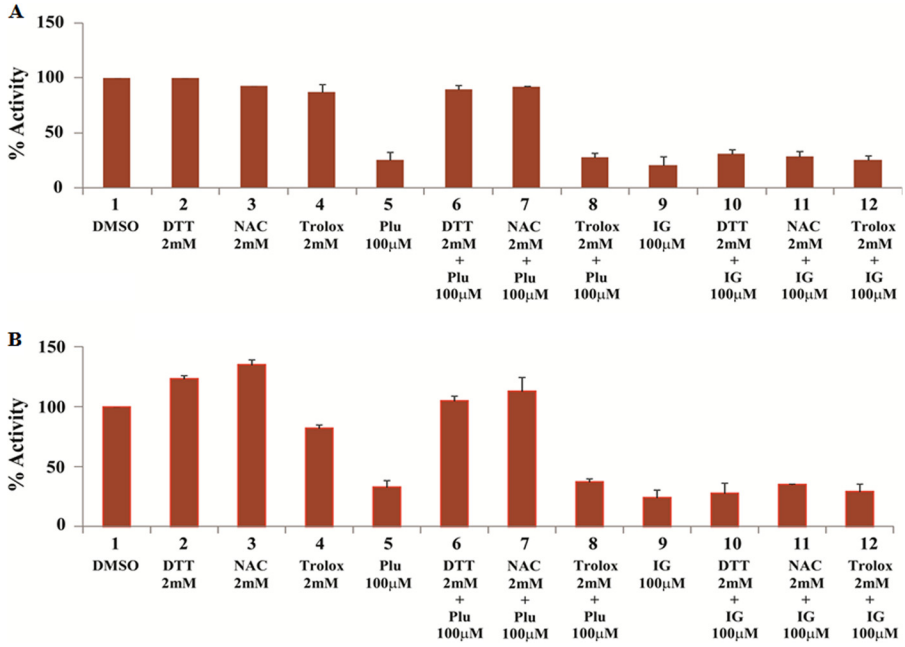

FIGURE 2. **NAC blocks plumbagin-mediated KAT inhibition *in vitro*.** Shown is the filter binding acetyltransferase assay using full-length baculovirus-expressed KATs, p300 (*A*), CBP (*B*), and HeLa core histones, with 100 μM plumbagin (*lanes 5–7* in *A and B*) or isogarcinol (*lanes 9–11* in *A and B*), either in the presence or absence of free-thiol-containing NAC and DTT. Filter-binding acetyltransferase assays were also performed with plumbagin and isogarcinol in the absence (*lanes 5* and *9*, respectively; *A* and *B*) or presence of the non-thiol reducing agent Trolox (*lanes 8* and *12*; *A and B*). *Error bars*, S.D.

due to the generation of ROS. DNA damage is marked by the predominance of histone H2AX phosphorylation (H2AXγ). We observed that 20 μM plumbagin drastically induced the level of H2AXγ (Fig. 1*B*, *lane 6*). Consistent with the absence of any visible cellular stress, pretreatment for 2 h with 2 mM NAC almost completely inhibited the plumbagin-induced DNA damage, as revealed by the near absence of H2AXγ even at an 80 μM concentration in SH-SY5Y and HeLa S3 cells (Fig. 1*B*, *lanes 3–5*). Remarkably, the KAT-inhibitory potential of plumbagin was completely abrogated in the presence of NAC (Fig. 1*C*, *lane 5 versus lanes 3* and *4*). However, the KAT-inhibitory activity of another broad spectrum KAT inhibitor, isogarcinol, remained unaffected in the presence of NAC (Fig. 1*D*). These observations imply two possible scenarios: 1) ROS induction leads to the inhibition of acetylation, and therefore NAC, through its free radical scavenging property, which could nullify ROS-mediated hypoacetylation, and 2) plumbagin reacts with free thiols in NAC, which abrogates KAT inhibition. However, the role of NAC as a free radical scavenger could not be ruled out from the experiments described above. We therefore performed the filter binding KAT assays *in vitro*. In this cell-free assay, plumbagin cannot generate H_2O_2 or superoxides. We observed that p300 and CBP inhibition by plumbagin are abrogated by NAC (Fig. 2, *A* and *B*, *lane 5 versus lane 7*). It was also observed that free thiol-containing reducing agents, such as DTT, have the same ability to abrogate both p300 and CBP KAT inhibition mediated by plumbagin (Fig. 2, *A* and *B*, *lane 5 versus lane 6*). However, non-thiol reducing agents, such as Trolox, did not affect plumbagin's KAT-inhibitory activity (Fig. 2, *A* and *B*, *lane 5 versus lane 8*). None of these reducing agents prevented isogarcinol from inhibiting KAT (Fig. 2, *A* and *B*, *lane 9 versus lanes 10–12*), suggesting that this phenomenon is unique to plumbagin. Therefore, thiol reactivity is critical in inducing toxicity and possibly contributed to KAT inhibition in cells.

Free Thiol Reactivity of Plumbagin Influences p300 Inhibition—Presumably, NAC reacted with plumbagin through its 3rd position. In addition, a reactive 3rd position may cause plumbagin-mediated toxicity due to enhanced redox cycling and free thiol reactivity. However, thiol reactivity of the molecule could influence the inhibition of acetyltransferase activity. We addressed this possibility through structure-activity relationship analysis. A variety of analogs of 1,4-naphthoquinone (Fig. 3*A*) were procured, and *in vitro* enzyme assays were performed with these compounds in the presence or absence of NAC (Fig. 4*A*). These small molecules vary substantially in their reactive potential at the 3rd position. It was observed that all of the analogs with a chemically reactive 3rd position (1,4-naphthoquinone, menadione, and 5-hydroxy-1,4-naphthalenedione (juglone) but not lawsone) inhibited p300 activity, albeit to varying extents. Lawsone did not show significant inhibition even at 100 μM. Although the inhibitory activities of thiol-reactive molecules such as 1,4-naphthoquinone were abrogated upon the addition of NAC (similar to the abrogation of plumbagin activity), this was not the case for juglone. Lawsone could not inhibit p300 significantly, and there was no further change after the addition of NAC (Fig. 4*A*). Considering that the hydroxyl group of plumbagin is crucial for p300 inhibition, it was interesting to note that other analogs without hydroxyl groups, such as 1,4-naphthoquinone, also inhibited p300. However 1,4-naphthoquinone possesses a reactive 3rd position that would enable reactivity to thiols. Thus, we presumed that the free thiol reactivity of these analogs with cysteines could influence their inhibitory activity. To correlate KAT inhibition and free thiol reactivity, we carried out a colorimetric assay for free thiol estimation using DTNB.

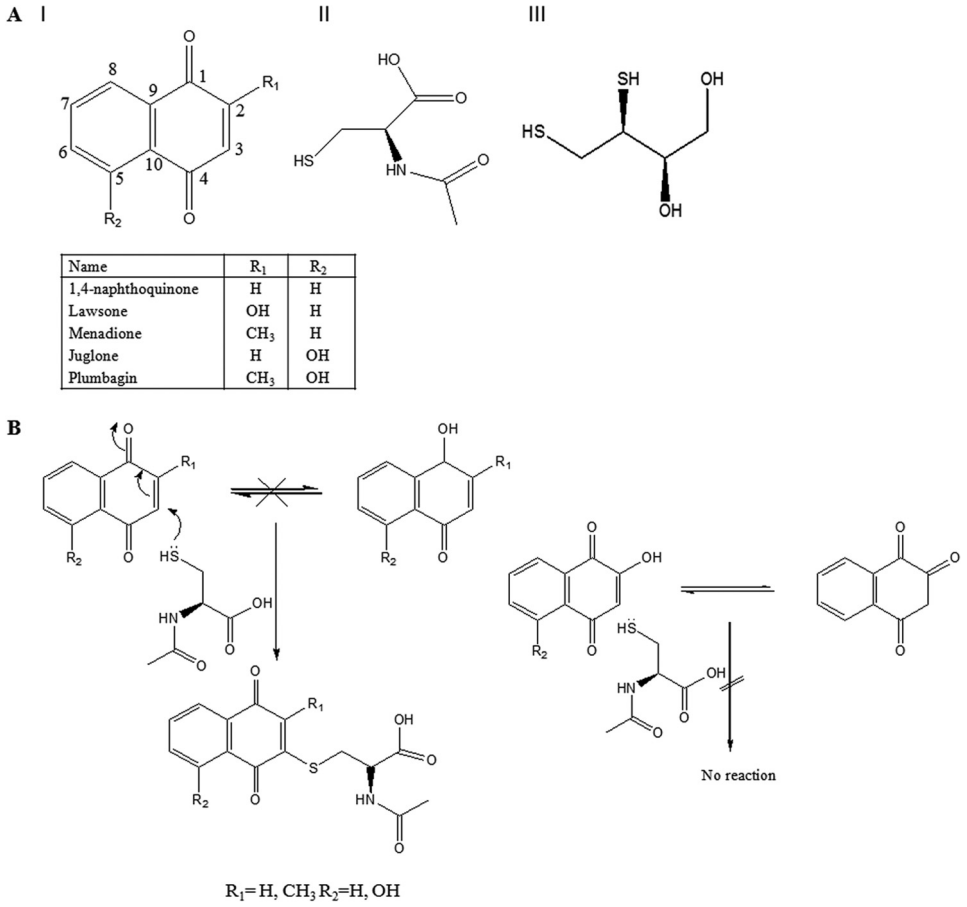

FIGURE 3. **Structures of 1,4-naphthoquinone analogs and reactive thiols.** *A*, structures of 1,4-naphthoquinone analogs (*I*), NAC (*II*), and DTT (*III*). The OH group at the 5th position in the case of plumbagin and juglone is very essential for the inhibition of p300 (see *table*). *B*, mechanism of NAC reactivity toward various analogs of 1,4-naphthoquinone. 1,4-Naphthoquinone analogs can react with thiol compounds like NAC/DTT due to the presence of a free electrophilic 3rd position in their generic structure. NAC is unable to react with lawsone due to keto-enol tautomerism.

The assay is based on the fact that the aromatic disulfide (DTNB) reacts with aliphatic thiol groups to form a mixed disulfide and 2-nitro-5-thiobenzoate. DTNB has negligible absorbance, but when it reacts with -SH groups under mild alkaline conditions (pH 7–8, physiological buffers), the 2-nitro-5-thiobenzoate anion (TNB^{2-}) gives an intense yellow color at 412 nm. Thus, if NAC covalently bound to any of the analogs of 1,4-naphthoquinone derivatives, the abundance of the free thiol group would be reduced, which would be reflected as a decrease in the absorbance. The NAC-mediated increase in absorbance was reduced by 1,4-naphthoquinone, plumbagin, and menadione at 50 μM, in all lanes containing NAC (Fig. 4*B*). An electron-donating group (hydroxyl group) occurs at the 5th position of plumbagin and is conjugated with the carbonyl group at the 4th position, which results in a diminished π-electron cloud around the C2=C3 double bond. This configuration leads to preferential nucleophilic attack at the 3rd position, and the structure is subsequently stabilized by the methyl group present at the 2nd position. In the absence of the electron-donating group (*i.e.* the methyl group), the symmetry would result in nucleophilic attack at either the 2nd or the 3rd position, as in the case of 1,4-naphthoquinone. However, in the case of menadione, which does not possess the hydroxyl group, the preferential position of nucleophilic attack is at the 3rd position because the 2nd position is occupied by a methyl group. The absence of a hydroxyl group at the 5th position coupled with a single site for nucleophilic addition is probably the reason that menadione is a weaker inhibitor than 1,4-naphthoquinone or plumbagin (Fig. 4*A*). In the case of juglone, the preferential mode of nucleophilic attack is at the 3rd position. However, the intermediate thus obtained is not as stable as that of plumbagin, and hence it results in poor affinity toward a nucleophilic attack, which can be correlated with a lack of a decrease in absorbance (Fig. 4*B*). In the case of lawsone, the 3rd position is highly nucleophilic in nature, which results in a decrease probability of NAC reacting with lawsone (Fig. 3*B*). Reactivity of 1,4-naphthoquinones to the free thiol group was also investigated using DTT, a different source of free thiol (Fig. 4*C*). Absorbance at 412 nm increased with increasing concentration of DTT. However, the increase was absent when 1,4-naphthoquinone, plumbagin, and menadione were present in the mixture at 50 μM. Consistent with previous observations, derivatives, such as lawsone and juglone, that do not react with NAC also do not alter the absorbance mediated by DTT. Lawsone and juglone did not react to DTT, whereas 1,4-naphthoquinone turned out to be the most reactive in terms of free thiol reactivity, followed by plumbagin and menadione (Fig. 4*C*). Because redox cycling could also influence the DTNB assay, direct reactivity of NAC with various derivatives of 1,4-naphthoquinone was confirmed by the UV-visible absorption spectra of these

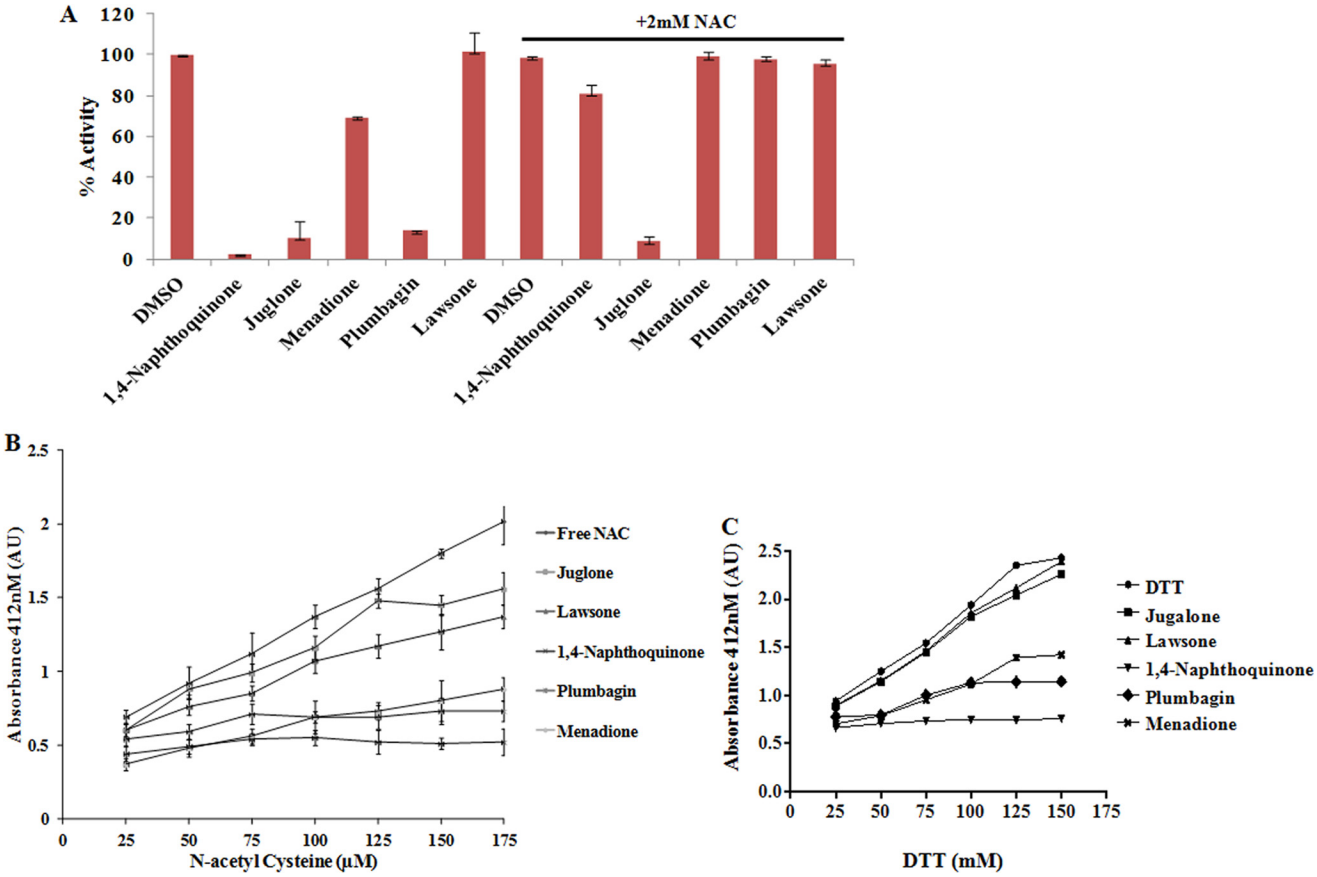

FIGURE 4. **Free thiol reactivity correlates with KAT-inhibitory properties of plumbagin analogs.** *A*, filter-binding acetyltransferase assays using full-length baculovirus-expressed p300 and HeLa core histones with 1,4-naphthoquinone, juglone, menadione, plumbagin, and lawsone (100 μM each) in the presence or absence of *N*-acetyl cysteine (2 mM). *B*, DTNB assay to assess the abundance of free thiols in different concentrations of NAC, after the addition of 1,4-naphthoquinone, juglone, menadione, plumbagin, and lawsone. *C*, DTNB assay to assess the abundance of free thiols in DTT after the addition of 1,4-naphthoquinone, juglone, menadione, plumbagin, and lawsone. *Error bars*, S.D.

compounds in the absence and presence of NAC (Fig. 5, *A–C*, *left panels*). The absorption spectra of plumbagin at 100 μM concentration showed an intense absorbance band at 271 and 420 nm. Upon the addition of NAC, the absorption spectrum showed a hypochromic shift to 246 and 426 nm. In the case of 1,4-naphthoquinone, two absorption bands were observed at 251 and 347 nm. The addition of NAC shifted the absorption bands toward a higher wavelength (*i.e.* 266 and 451 nm). Similarly, in the case of menadione, the UV-visible spectrum showed three bands at 251, 265, and 345 nm, which upon the addition of NAC again shifted toward higher wavelengths of 260, 341, and 438 nm, respectively. These results indicated that the π-electron cloud is disturbed around the compounds due to the addition of NAC, which may be a result of NAC reacting directly with these molecules. The result of NAC reacting with the various derivatives of plumbagin was further reflected in the changes in the fluorescence emission spectra of these molecules (Fig. 5, *A–C*, *right panels*). Plumbagin exhibited an emission band at ~449 nm. The intensity of the emission spectra showed a drastic increase in intensity upon the addition of NAC. A highly intense emission band was also observed at 505 nm. In the case of 1,4-naphthoquinone, an intense emission band was observed at ~438 nm, which disappears completely upon the addition of NAC. Similarly, in the case of menadione, the emission band at 435 nm disappeared completely upon the addition of NAC. These results clearly indicate that the direct reaction of NAC with 1,4-naphthoquinone derivatives results in a drastic change in the electronic environment around the molecules, thereby altering their emission and absorption spectra. These results, in addition to those obtained with the DTNB assay, clearly indicate that NAC reacts with these molecules through its free thiol at the 3rd position of the molecules. Additionally, these molecules, except juglone, react with NAC and thereby inhibit KAT activity.

PTK1, a Plumbagin Analog, Inhibits KAT Activity Independently of Free Thiol Reactivity—Based on earlier observations, we hypothesized that, if the reactivity at the 3rd position could be nullified while maintaining the hydroxyl group at the 5th position, then it could be possible to synthesize a non-toxic KAT inhibitor. Thus, we synthesized PTK1, with a methyl substitution at the 3rd position of plumbagin (Fig. 6*A*). Remarkably, it was observed that the ability of PTK1 to inhibit KAT was insensitive to the presence of NAC *in vitro* (Fig. 6*B*). As expected, in the DTNB-based assay for free thiol, the presence of PTK1 did not significantly affect free thiol abundance in the reaction containing NAC (Fig. 6*C*). Fluorescence emission as well as the UV-visible absorption spectrum of PTK1 were analyzed to investigate any covalent interaction with free thiol (Fig. 6*D*). Unlike other analogs, the PTK1 absorption band at 249 nm was not affected at all upon the addition of NAC. PTK1 showed no

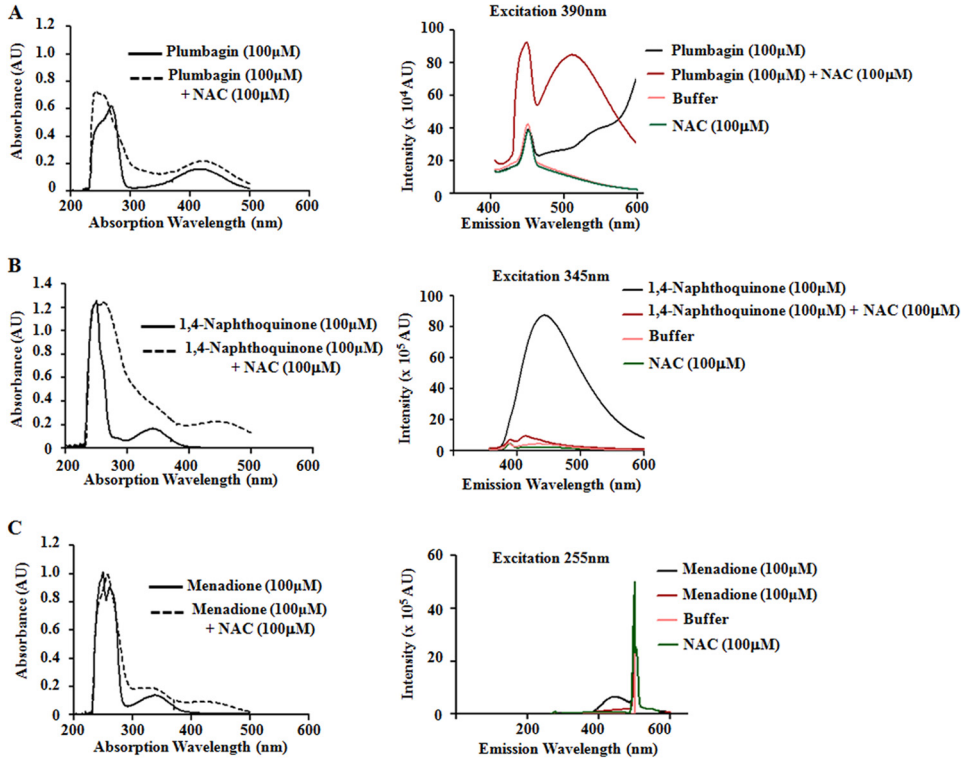

FIGURE 5. **NAC reactivity influences the absorption and emission spectrum of 1,4-naphthoquinone analogs.** *A*, UV-visible absorption spectra of plumbagin in the presence or absence of NAC (*left*) and fluorescence emission spectra of plumbagin in the presence or absence of NAC (*right*). *B*, UV-visible absorption spectra of 1,4-naphthoquinone in the presence or absence of NAC (*left*) and fluorescence emission spectra of 1,4-naphthoquinone in the presence or absence of NAC (*right*). *C*, UV-visible absorption spectra of menadione in the presence or absence of NAC (*left*) and fluorescence emission spectra of menadione in the presence or absence of NAC (*right*). In all cases, the concentrations of the inhibitors and reducing agent used are indicated.

fluorescence emission spectra, and consequently, the changes with NAC addition could not be monitored. Moreover, this derivative exhibited the same *in vitro* KAT inhibition potency as the parent compound plumbagin (data not shown). To ascertain the inhibition of histone acetylation in cells, we performed immunoblotting with lysates of SH-SY5Y, HEK293, and HeLa S3 cells treated with PTK1 at different concentrations using an H3K9 acetylation antibody. We observed a dose-dependent decrease in acetylation after 24 h of treatment (Fig. 6*E*, *lane 1 versus lanes 2–5*). Collectively, these results suggest that PTK1 is a KAT inhibitor whose activity is independent of free thiol reactivity.

PTK1 Is a Non-competitive and Reversible Inhibitor of p300—The kinetic analysis of the PTK1-mediated inhibition of full-length p300 acetyltransferase revealed a noncompetitive pattern with both of its substrates (*i.e.* core histones and [^{3}H]acetyl-CoA) (Fig. 7, *A* and *B*). The Lineweaver-Burk plots (Fig. 7, *A* and *B*, *left panels*) at a fixed substrate concentration revealed that apparent K_m values (1.47 ± 0.2 μM for acetyl-CoA and 33.33 ± 2 nM for core histone) remained constant while the V_{max} of the enzyme decreased with increasing concentration of PTK1 (from 8476 ± 268.2 cpm without inhibitors to 3184 ± 125.6 cpm with 45 μM PTK1 for acetyl-CoA and from 4732 ± 36.52 cpm without inhibitors to 2077 ± 27.16 cpm with 45 μM PTK1 for core histone). We also observed a significant increase in both the slope (K_m/V_{max}) and the *y* intercept (when $x = 0.0$) by the same factor (2.7-fold for acetyl-CoA and 2.5-fold for core histone), which distinguishes between inhibition by classical noncompetitive kinetics and mixed kinetics. The slopes (K_m/V_{max}) obtained were further plotted against inhibitor concentrations to determine the K_i (inhibitor constant) value. The K_i of PTK1 was determined to be 23 μM for acetyl-CoA ($R^2 > 0.98$; $p < 0.0001$) and 30 μM for core histone ($R^2 > 0.98$; $p = 0.0002$) (Fig. 7, *A* and *B*, *middle panels*). To further validate the steady-state kinetics data, they were also analyzed by a secondary plot (Fig. 7, *A* and *B*, *right panels*), where 1/apparent maximum velocities ($1/V_{app}$) from Lineweaver-Burk plot were plotted against the PTK1 concentrations, and the K_i' values were found to be 23 and 30 μM for acetyl-CoA and core histones, respectively. The identical K_i and K_i' values clearly suggest a purely non-competitive mechanism of inhibition. Additionally, the values are comparable with the inhibition constant of plumbagin (20–25 μM) (4) and strengthen the hypothesis that PTK1 possesses the same inhibition potency *in vitro* as the parent plumbagin molecule. These findings are not surprising, considering that PTK1 is a methylated derivative of plumbagin, and the parent molecule inhibits full-length p300 as well as the minimal KAT domain by a noncompetitive mechanism (4). Bisubstrate enzymes, such as p300, follow an ordered substrate binding mechanism (31). The non-competitive inhibitor PTK1 could bind to the free enzyme as well as to the substrate-bound form, resulting in an abortive ternary complex. The possibility of a conformational change due to allosteric binding also cannot be ruled out. In addition, PTK1 may have multiple or partially overlapping binding sites in the biologically relevant full-length p300.

To investigate and compare the reversibility of the plumbagin and PTK1-mediated inhibition, we performed dialysis in

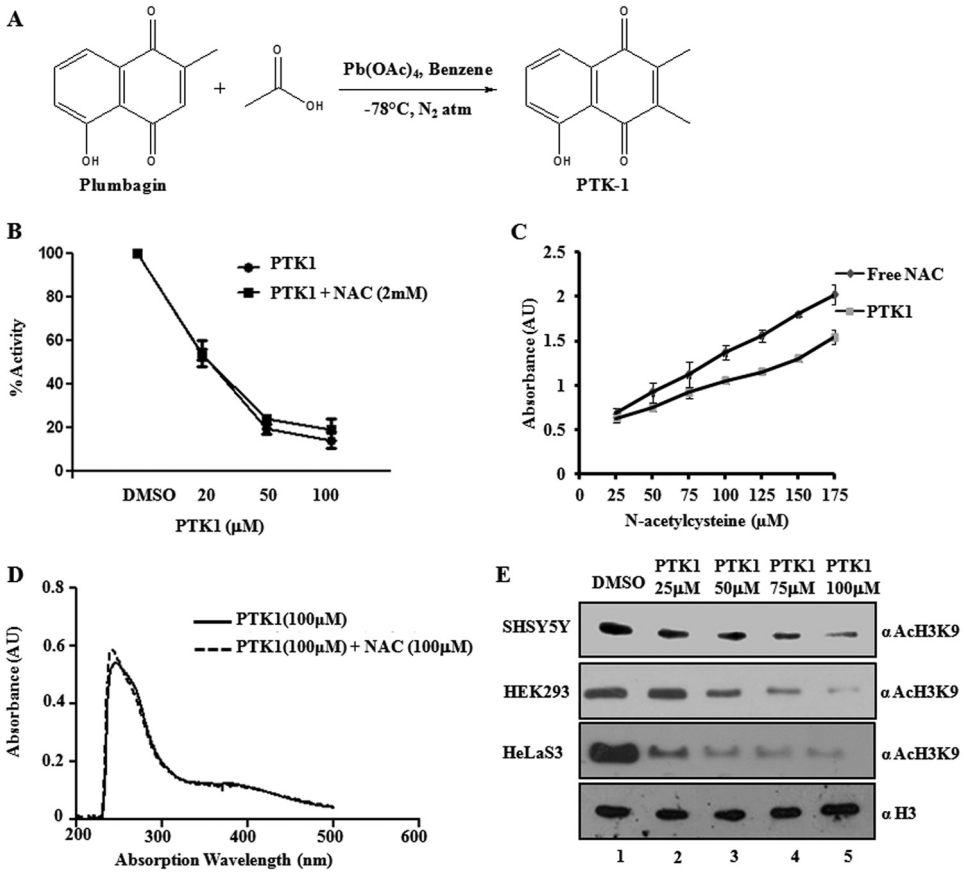

FIGURE 6. **PTK1 inhibits p300 independently of free thiol reactivity.** *A*, synthesis of PTK1 from plumbagin. *B*, filter binding acetyltransferase assays using full-length baculovirus expressed p300 and HeLa core histones with different concentrations of PTK1 in the absence and presence of NAC. *C*, *in vitro* DTNB assay to assess the abundance of free thiol in the presence or absence of PTK1. *D*, UV-visible absorption spectrum of PTK1 in the in presence or absence of NAC. *E*, immunoblotting analysis (*IB*) of cell lysates upon 24 h of treatment by PTK1 using H3K9 acetylation antibodies. The concentrations of PTK1 used are indicated in the figure. *Error bars*, S.D.

addition to dilution-based time course inhibition assays (Fig. 8). In these assays, an indication of reversibility is the independence of inhibition with respect to time. Perfectly reversible inhibitors reach rapid equilibrium with the enzyme, and inhibition does not depend on time. Plumbagin exhibited perfect time-dependent inhibition at a range of concentrations (25–100 μM) with 1–15 min of preincubation. Inhibition markedly increased with the time of incubation with the inhibitor. The inactivation rate constant (k_{obs}) value was determined from the fitted slope of the plots; for plumbagin, it was 4×10^{-2}/min (Fig. 8*A*, *left*). This type of inhibition is usually the result of the irreversible binding of the inhibitor with the enzyme, potentially due to the formation of covalent adducts. In the case of plumbagin, it could be due to the complex-forming ability of selective thiol residues in the protein. The irreversibility of plumbagin-mediated inhibition was further confirmed by the rapid "drop dialysis" method, in which dialysis of plumbagin was ineffective in restoring the native activity of the enzyme (Fig. 8*B*). This scenario changed when PTK1 was used; we observed minimal time-dependent decrease when compared with the without inhibitor control ($k_{obs} = 9 \times 10^{-3}$/min) (Fig. 8*A*, *right*). Moreover, the inhibition of PTK1 was completely reversible because complete activity could be recovered after determining the residual activity of the dialyzed enzyme, which was free from PTK1 (Fig. 8*B*). These data suggest that the mechanism of inhibition of p300 by plumbagin is irreversible, whereas for PTK1, it is predominantly reversible. Importantly, when these assays were conducted with the minimal p300 KAT domain (Fig. 8*C*), both small molecules behaved in a totally reversible fashion with no time dependence and completely regained their activity upon dilution (Fig. 8*D*). This result also suggested that the susceptibility to redox cycling and free thiol reactivity resides in residues outside the KAT domain, presumably in the cysteine- and histidine-rich domains of the full-length enzyme.

The Binding Sites for Plumbagin and PTK1 Are Probably the Same within the KAT Domain—It was previously found that plumbagin could bind to only one site within the KAT domain of p300, namely, the Lys-1358 residue, by isothermal titration calorimetry, molecular docking, and mutation studies (4). A detailed kinetic analysis also revealed a non-competitive mechanism of inhibition of both the full-length protein and the KAT domain. To assess whether the binding site for PTK1 was similar to that of plumbagin, we performed molecular docking using Autodock software (Fig. 9*A*). The docking study with PTK1 and the p300 KAT domain showed hydrogen bond formation with residue Lys-1358 (Fig. 9*B*). The residues involved in the interaction were Lys-1358, Arg-1356, Thr-1296, Leu-1298, Glu-1380, Asp-1614, and Asp-1616 (Fig. 9*C*). This docking model is consistent with the aforementioned report (4) in

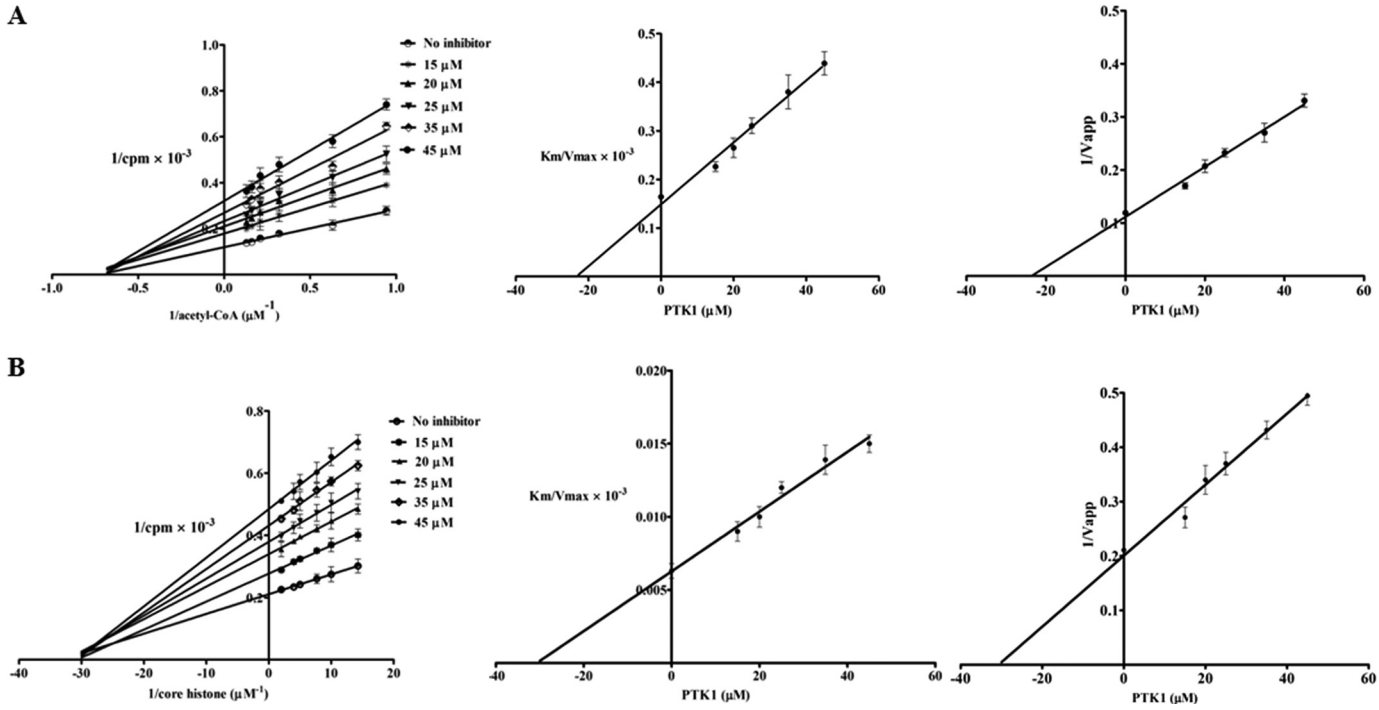

FIGURE 7. **PTK1 is a noncompetitive inhibitor of p300.** *A*, kinetics of p300 KAT inhibition by PTK1 as represented by a Lineweaver-Burk plot (*top left*). The concentration of core histones has been kept constant at 1.7 μM while increasing the concentration of [^{3}H]acetyl-CoA from 1 to 8 μM either in the absence (no inhibitor) or increasing concentrations of PTK1 (15, 20, 25, 35, and 45 μM). In order to determine the K_i of PTK1 for acetyl-CoA, the slope (K_m/V_{max}) of the straight lines obtained from the Lineweaver-Burk plot is plotted against PTK1 concentrations (*top middle*). The apparent V_{max} values from the Lineweaver-Burk plot are plotted against PTK1 concentrations (*top right*). *B*, inhibition of p300 KAT activity by PTK1 at a fixed concentration of [^{3}H]acetyl-CoA (1.6 μM) and increasing concentrations of core histones (5–70 nM) either in the absence of (no inhibitor) or increasing concentrations of PTK1 (15, 20, 25, 35, and 45 μM). Data are represented by a Lineweaver-Burk plot (*bottom left*). In order to determine the K_i of PTK1 for core histone, the slope (K_m/V_{max}) of the straight lines obtained from the Lineweaver-Burk plot is plotted against PTK1 concentrations (*bottom middle*). The apparent V_{max} values from the Lineweaver-Burk plot are also plotted against PTK1 concentrations. (*bottom right*). *Error bars*, S.D.

which it was shown that the -OH group of plumbagin, which has a structure similar to that of PTK1 (without the methyl group at C3), is important because plumbagin forms a hydrogen bond with Lys-1358 through this group. It had also been shown that alkyl substitution at the -OH position could not inhibit KAT activity. Additionally, Lys-1358 was found to be absolutely critical for KAT activity. A hydrogen bond is formed with the Arg-1356 residue, and, along with the hydrogen bond formed with Lys-1358, it could facilitate interactions with the other four residues. The docking of PTK1 with the p300 KAT domain suggested that hydrogen bonding through the -OH group of the molecule to the Lys-1358 residue could result in the inhibition of KAT activity. Therefore, we observed that PTK1 probably bound to the same region as plumbagin and possibly followed a similar mechanism for inhibition of KAT activity. The docking results are consistent with this conclusion but certainly not conclusive.

Plumbagin Induces p300 Structural Alterations by Inducing Thiol Cross-links and Adduct Formation—Plumbagin and 1,4-naphthoquinone share a reactive 3rd position, which could induce both redox cycling and covalent thiol adduct formation. Redox cycling *in vitro* can induce many changes in proteins. The induction of thiol cross-links between cysteine residues is one such effect. p300 has three cysteine- and histidine-rich regions (CH1, CH2, and CH3) and therefore is likely to be affected by redox states. CH2 and CH3 are adjacent to the KAT domain. It is possible that redox cycling induces disulfide bonds in an intermolecular or intramolecular fashion, thereby contributing to KAT inhibition. Full-length p300 is a 300-kilodalton protein (Fig. 10*A*), and induction of such cross-links can result in dimerization or oligomerization, which in turn result in a drastic increase in the protein size. This size increase can be observed as reduced mobility in SDS-PAGE (without DTT). As expected, after preincubation with plumbagin analogs (25 or 100 μM), there is a variable decrease in mobility (Fig. 10*B*, *lane 1 versus lanes 2–5*). The decrease in mobility correlates with increased protein sequestration at the interface of the stacking gel and the resolving gel as observed upon Coomassie Blue staining. This sequestration was due to a drastic increase in size, which was possibly a result of dimer-/oligomerization by thiol cross-links. Interestingly, PTK1 and juglone induced dimer-/oligomerization to a lesser extent than plumbagin at both concentrations. A reactive 3rd position probably enhances redox cycling to some extent. As expected, the presence of DTT greatly reduced the dimer-/oligomerization. It is possible that dimer-/oligomerization induced by redox cycling of 1,4-naphthoquinones contributes to KAT inhibition. PTK1 therefore possesses a limited ability to induce p300 intra-/intermolecular thiol cross-links. The thiol-cross-linking abilities of the three compounds were also compared by a dynamic light scattering experiment. The results suggest the following features (Fig. 10*C*). Plumbagin induced oligomerization of p300 to a greater extent relative to PTK1 and juglone, because the Z_{av} diameter of untreated p300 (99.9 nm) increased to 161.1 nm in the pres-

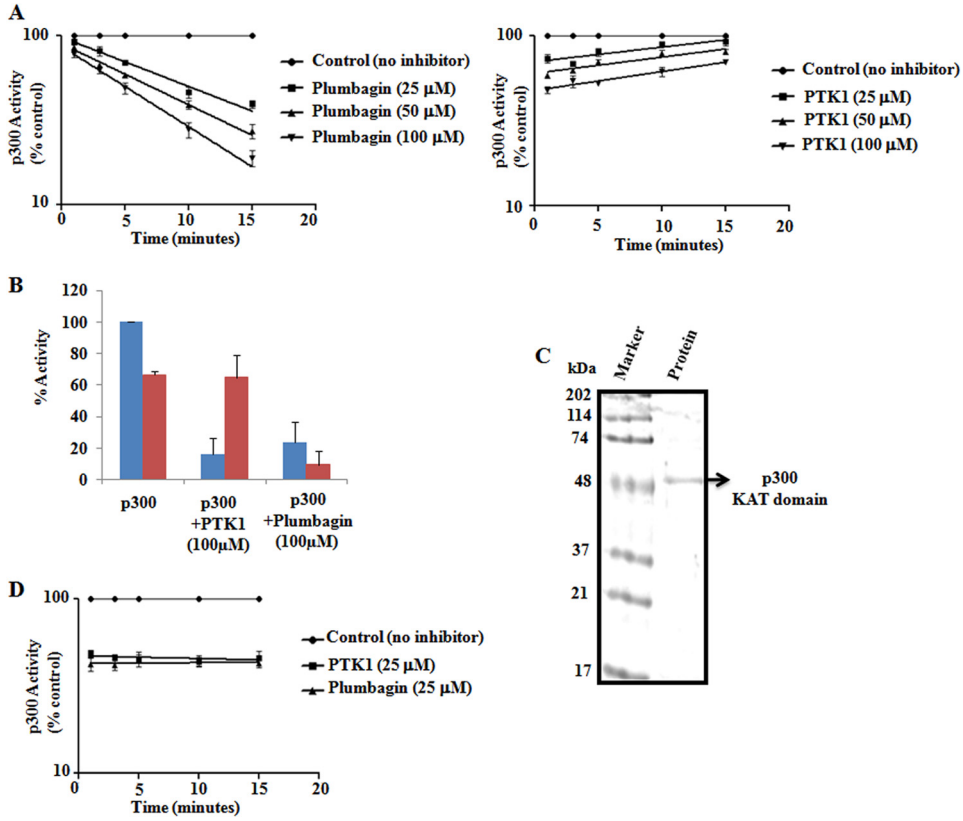

FIGURE 8. **Reversibility of the inhibition of p300 by plumbagin and PTK1.** *A*, the time-dependent inhibition of p300 by plumbagin. Semilogarithmic plots showing the time-dependent inactivation of various concentrations of plumbagin (*left*) and PTK1 (*right*), as indicated. The results are presented as the mean ± S.D. of triplicate measurements. The residual activity is shown as a percentage of control (without inhibitor) as described under "Experimental Procedures." The data were fitted against the preincubation time using the semilog line (*x* is log, *y* is linear) module of GraphPad Prism version 5.0. The time-dependent inactivation constant, k_{obs}, was obtained from the semilogarithmic plots of the residual activity. *B*, dialysis was carried out by incubating p300 with inhibitors for 30 min, and the mixture was dialyzed at 4 °C against 2× HAT assay buffer. The residual activity was assayed and compared with predialysis activity. The values were mean ± S.D. of three independent measurements. *C*, purification profile of recombinant p300 KAT domain expressed in *Escherichia coli*. Purified protein was visualized in 12% SDS-polyacrylamide gel and stained with Coomassie Brilliant Blue. *D*, time-dependent inhibition of p300 with 25 μM plumbagin and PTK1 using the p300 KAT domain with compound preincubation times ranging from 1 to 15 min as described earlier.

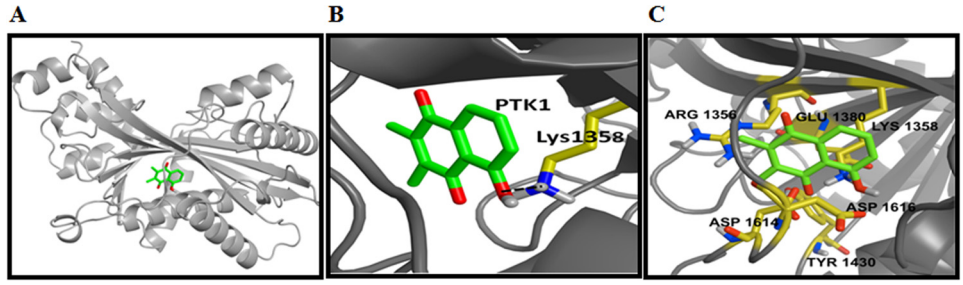

FIGURE 9. **Molecular docking revealed that PTK1 has same binding site as plumbagin.** *A*, docking of PTK1 (shown in a *stick representation*) onto the p300 KAT domain (shown in a *cartoon representation*). The crystal structure of the p300 KAT domain was extracted from the Protein Data Bank using the code 3BIY. *B*, hydrogen bonding of the PTK1 molecule with the Lys-1358 residue (hydrogen bond length 2.51 Å, shown as a *dotted line*). *C*, the docking conformation of the PTK1 molecule (carbon, oxygen, and hydrogen atoms are *colored* in *green*, *red*, and *white*, respectively) and surrounding residues in hydrophobic contact (carbon, nitrogen, and oxygen atoms are *colored* in *yellow*, *blue*, and *white*, respectively).

ence of 25 μM plumbagin (Fig. 10*C*, *top*). The further addition of plumbagin (100 μM) did not cause any significant change in the Z_{av} diameter of p300. However, in the presence of 25 μM PTK1 or juglone, Z_{av} was found to be ~121 nm. This value increased to ~129 nm in the presence of these compounds at 100 μM. The Z_{av} diameter trends clearly reflected the differential cross-linking abilities of plumbagin *versus* PTK1 and juglone (Fig. 10*C*, *top* and *bottom*). The statistical analysis also supported the aggregation of p300 in the presence of the three compounds (data not shown). However, the extent of aggregation follows the following order: plumbagin > PTK1 ~ juglone. These results further corroborate the findings from the gel electrophoresis data.

To understand the structural changes in p300 (KAT3B) induced by plumbagin and PTK1, we used SERS analysis, which has been a very effective and quick technique used to look for gross protein structure. SERS is a unique approach to monitor structural changes in enzymes such as p300 upon the binding of

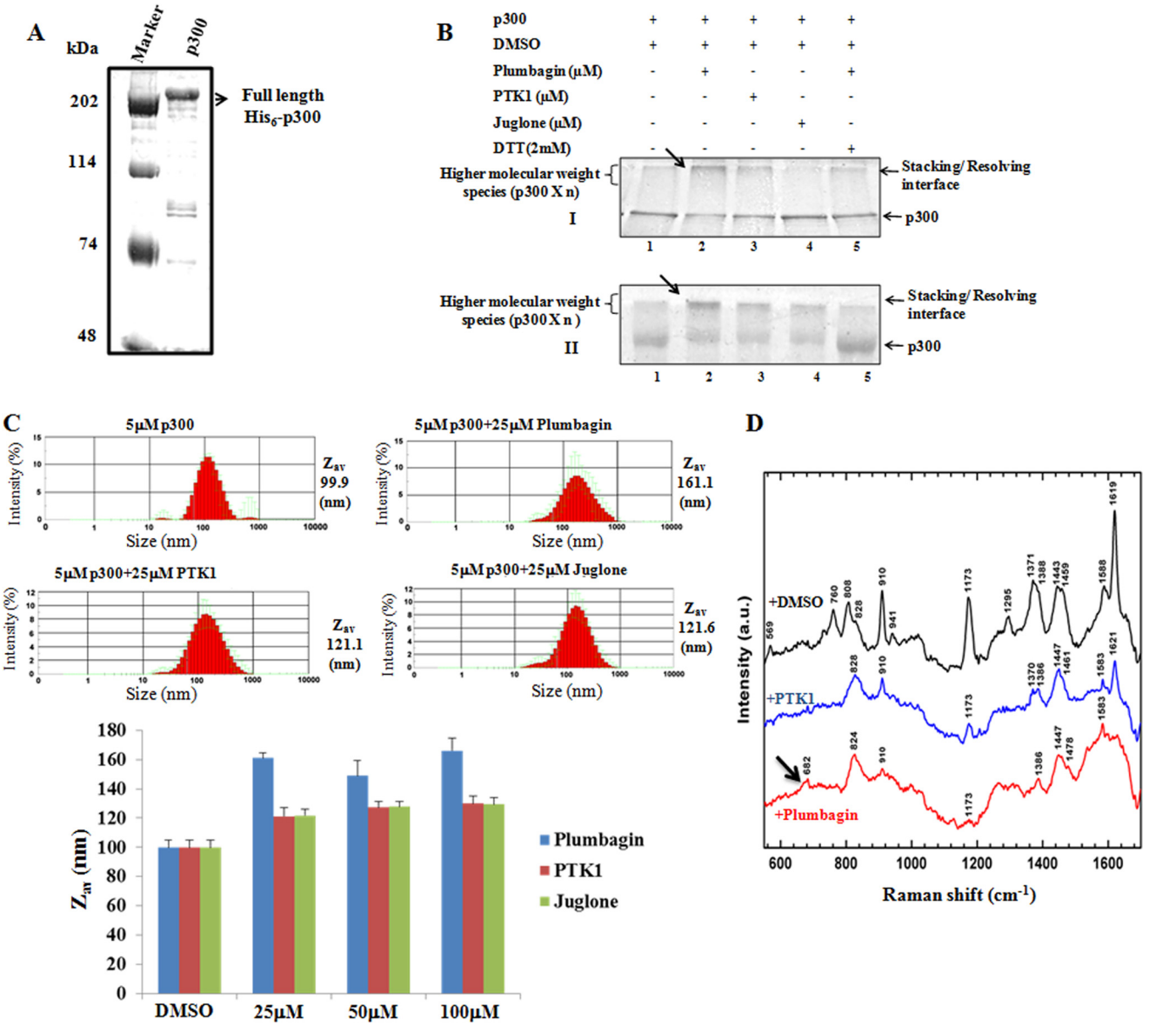

FIGURE 10. **p300 undergoes thiol cross-links and adduct formation under redox stress *in vitro*.** *A*, purification profile of recombinant full-length baculo-expressed p300. The protein was loaded in 8% SDS-polyacrylamide gel and stained with Coomassie Brilliant Blue stain. *B*, p300 was incubated with various 1,4-naphthoquinone analogs with 25 μM (*I*) and 100 μM (*II*) for 10 min at 30 °C and subjected to SDS-PAGE without DTT. The gel was stained with Coomassie Brilliant Blue, including the stacking/resolving interface. The *heavy black arrow* indicates oligomeric p300 in the presence of plumbagin (*lane 2*). *C*, dynamic light scattering to study the influence of plumbagin, PTK1, and juglone on p300 dimer-/oligomerization. The intensity statistics of 10 measurements each are plotted for p300 (5 μM) alone and in the presence of 25 μM plumbagin, PTK1, and juglone, respectively (*top*). The Z_{av} diameters are listed on each *panel*. Shown are Z_{av} diameters for p300 (5 μM) treated with 25, 50, and 100 μM plumbagin, PTK1, and juglone, with *error bars* indicating S.D. (*bottom*). The measurements were performed at 25 °C. *D*, SERS spectra of p300 alone (*black*), p300 with PTK1 (*blue*), and p300 with plumbagin (*red*).

ligands (32–34). These structural changes alter the orientation of the rings of aromatic amino acids with respect to the nanoparticle surface and thus alter the enhancement of different ring modes of these amino acids. In addition, the binding of the ligand can distance the metal nanoparticle's surface from that of the protein, resulting in a reduction in intensity or the disappearance of the associated Raman modes. In cases where ligands do not bind to the protein, the SERS spectrum of the protein does not show any changes. SERS is a very sensitive method, and the spectra of the proteins depend on the distance and orientation of the protein on the surface of the nanoparticles. Therefore, this technique gives us insight into the structural changes upon the binding of ligands to proteins (35). The spectra of baculo-expressed full-length p300 (Fig. 10*A*) treated with plumbagin or PTK1 underwent such changes (Fig. 10*D*). The tentative SERS band assignments of p300 were performed as described previously (15, 32, 34, 36). The band at 1619 cm^{-1}, which is the amide I mode, diminished moderately in intensity in the case of PTK1 and almost completely disappeared in the case of plumbagin. This result suggested that the binding of the molecules to the protein took place predominantly in the α-helix or β-sheet regions. The change in amide I band intensity directly correlated with the extent of interactions of the compounds with the protein, which resulted in structural changes. The amide III band occurring at 1295 cm^{-1} also diminished in intensity, showing binding of the molecules to the secondary

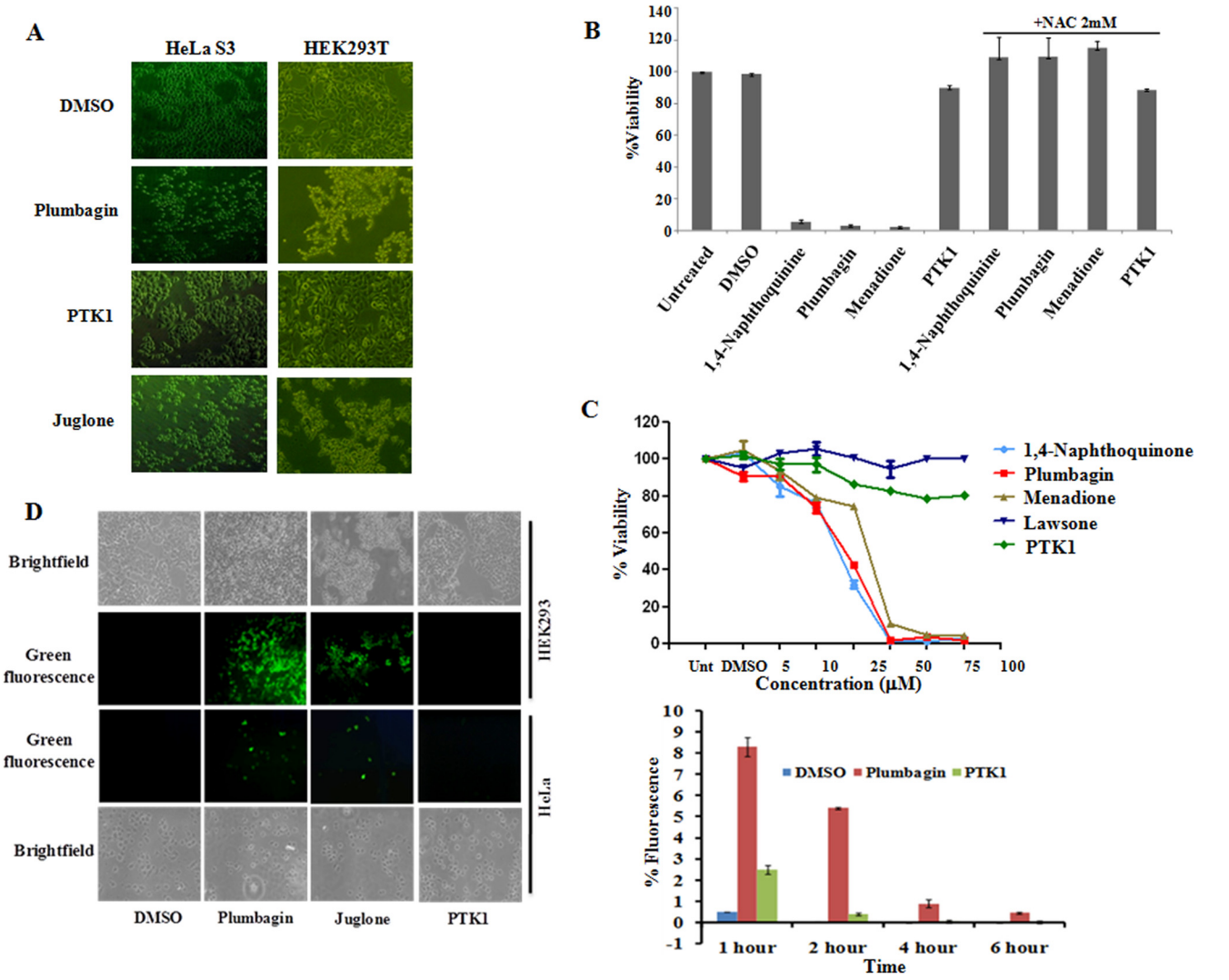

FIGURE 11. **PTK1 has a greatly improved toxicity profile.** *A*, HeLa S3 cells were treated with 40 μM plumbagin, PTK1, and juglone for 6 h, and microscopic images were captured (*left*). HEK293 cells were treated with 50 μM plumbagin, PTK1, and juglone for 6 h, and microscopic images were captured (*right*). DMSO-treated cells were used as a control. *B*, MTT assay to estimate cell viability with 1,4-naphthoquinone analogs either alone or with NAC pretreatment after 24 h in the SH-SY5Y cell line; *C*, MTT assay to compare cell viability upon treatment of HeLa S3 cells with 1,4-naphthoquinone analogs and PTK1. The concentration of the analogs used is indicated in the figure. *D*, CM-H2DCFDA fluorescent images of HEK293 and HeLa cells obtained after administration of 25 μM plumbagin, juglone, and PTK1 for 2 h. An equal volume of DMSO was used as solvent control. Bright field images were taken to monitor cellular morphology after the treatment (*left*). HeLa cells were administrated with 50 μM plumbagin (*red*) and PTK1 (*green*) for the indicated time period, and DCF fluorescence was quantified by flow cytometry (*right*). An equal volume of DMSO (*blue*) was used as a solvent control. *Error bars*, S.D.

structure of the protein. For both PTK1 and plumbagin, there were changes in the intensities of the bands in the 1150–1550 cm^{-1} region that were related to the aromatic amino acids tryptophan, tyrosine, phenylalanine, and histidine, whose orientations with respect to the nanoparticle surface changed upon binding of the molecules to the protein. In the case of the p300 protein, we observed the stretching vibrations of C-COO^- as a doublet at 910–941 cm^{-1}. The presence of this doublet indicated that the protein interacted with the silver nanoparticles predominantly through the carboxylate groups. However, the intensity of the doublet decreased in the case of PTK1 and almost completely disappeared in the case of plumbagin. Plumbagin also possesses an intrinsic tendency to bind to free thiol groups on the surface of the protein through nucleophilic addition to the C3 carbon. This result was confirmed by the appearance of a peak at 682 cm^{-1}, which corresponds to the ν_s(C-S-C) mode (37). This mode was absent in free protein and protein-PTK1 spectra. The appearance of this mode specifically when plumbagin was applied to p300 gave absolute evidence that protein-small molecule thiol adducts were being formed. The nonspecific binding of plumbagin to the protein surface could also prevent nanoparticles from binding to the protein or change the binding site, thereby causing an overall reduction in intensities of different modes like the C-COO^- stretching modes.

PTK1 Has a Greatly Improved Toxicity Profile—Based on the observation that 1,4-naphthoquinone derivatives reacted with NAC at their free 3rd position, we hypothesized that this mode of reaction between the molecules and various free thiols present within the cell could explain their high toxicity. We found that the application of plumbagin and juglone but not PTK1 at different concentrations in HeLa S3 and HEK293 cells induced drastic changes (Fig. 11*A*). Thus, when there was an excess of

free thiols added to the cell culture medium (NAC or DTT), indiscriminate binding of 1,4-naphthoquinone analogs to cellular thiols and proteins was avoided. Therefore, we performed an MTT assay with 1,4-naphthoquinone analogs that react with NAC to score their toxicity in the SH-SY5Y cell line (Fig. 11*B*). All of the molecules that bound to free thiols were highly toxic, resulting in nearly zero viability at 75 μM treatment for 24 h. Excess NAC totally abrogated the analogs' toxicity even at an otherwise lethal dose of 75 μM, suggesting that reactivity at the 3rd position leads to free thiol reactivity, which caused KAT inhibition as well as toxicity. Therefore, when we compared PTK1 with these derivatives, the toxicity was greatly reduced. Even at 75 μM, when other analogs with reactive 3rd positions caused nearly 100% cell death, PTK1 caused only 20% cell death upon a 24-h treatment (Fig. 11*C*). Therefore, among the 1,4-naphthoquinone KAT inhibitor analogs, PTK1 stood out as nearly non-toxic. Because the toxicity level of PTK1 was greatly reduced, we examined the ROS generation ability of PTK1. We found that PTK1 had almost lost the ability to generate ROS, whereas both plumbagin and juglone generated reactive oxygen species, as detected by the accumulation of the oxidized fluorescent product DCF inside the cells upon exposure to CM-H2DCFDA (a cell-permeable, non-fluorescent precursor of DCF) (Fig. 11*D*, *left*). A time course comparison of ROS induction between plumbagin and PTK1 revealed that PTK1 has a drastically reduced ability to generate ROS (Fig. 11*D*, *right*). As quantified by the accumulation of fluorescence in the cell, the number of fluorescent cells further decreased over the monitored time period.

DISCUSSION

Small molecule modulators of lysine acetyltransferases have recently received enthusiastic attention because they may help us to understand *in vivo* KAT function. They also possess tremendous potential as molecules for therapy. Here, we have described our effort to understand the mechanism of action of a class of KAT inhibitors (naphthoquinones), some of which interact with thiols in addition to the KAT domain of p300. The detailed functional analyses of these molecules led to the identification of the chemical entity responsible for KAT inhibition and cellular toxicity. Based on this information, we have synthesized a new inhibitor, PTK1, which does not react with thiols and inhibits KATs in a non-competitive and completely reversible fashion. In comparison with other analogs, it exhibits reduced ROS generation. Therefore, PTK1 is a non-toxic KAT inhibitor.

Plumbagin is an antiproliferative and cytotoxic compound (38). We have investigated the mechanism responsible for toxicity and have identified that the reactive 3rd position is essential for toxicity. Furthermore, through its free thiol reactivity, plumbagin influences p300/CBP KAT inhibition. The contribution of free thiol reactivity to KAT inhibition has also been suggested for the isothiazone-mediated inhibition of p300/CBP-associated factor and p300 (39). We previously reported that the inhibition of KAT activity by plumbagin is may be due to hydrogen bonding of the single hydroxyl group at the 5th position to a critical lysine residue within the KAT domain of p300 (4). This concept has been further strengthened by the observation that one of the analogs, juglone (5-hydroxy-2-methyl-1,4 naphthoquinone), which possesses only one hydroxyl group and does not possess thiol reactivity, greatly inhibits the KAT activity of p300. Furthermore, our data clearly suggest that the abilities of plumbagin with regard to redox cycling and the formation of adducts with the enzyme result in the toxicity of this molecule.

Based on this structure-function information about plumbagin, we synthesized a derivative, PTK1 that, because of a methyl substitution at the 3rd position, does not react with thiols. PTK1 possesses a hydroxyl group at the 5th position, which probably maintains its KAT-inhibitory activity. Although PTK1 showed an IC_{50} value similar to that of plumbagin *in vitro*, its inhibition of H3K9 acetylation in the cell lines was approximately half that of plumbagin. We propose two possibilities for this differential efficiency of PTK1 and plumbagin in the cellular system: 1) cellular permeability is low for PTK1 compared with plumbagin; 2) because plumbagin forms an adduct with the enzyme, it inhibits the enzyme's activity more strongly than does PTK1. ROS generated by plumbagin could also induce thiol cross-links in the enzyme, thus reducing its activity in the cellular context.

NAC is able to bind to a wide array of molecules, including 18β-glycyrrhetinic acid derivatives, and thus prevent apoptosis (40). Additionally, NAC prevents plumbagin-dependent inhibition of the NFκB pathway in a free thiol-dependent manner via inhibition of the association between plumbagin and p65, a key subunit of the NFκB p50/p65 heterodimer complex (25). NAC and other free thiol-containing reducing agents, but not the non-free thiol-reducing agents, modify the immunomodulatory activity of plumbagin (26). Apoptosis induced by 1,4-naphthoquinone analogs, such as plumbagin, can be completely blocked by NAC but not by the non-free thiol-containing reducing agents (27). From our study, it is clear that NAC can completely abrogate the toxicity of plumbagin and its analogs not only by scavenging ROS (25, 26, 39) but also by reacting with them directly in a cellular system. Collectively, thiol donors, such as NAC and DTT, render the 1,4-naphthoquinones chemically inert.

In conclusion, we have addressed the chemical mechanisms that could be involved in influencing KAT inhibition by 1,4-naphthoquinone, and we have delineated thiol reactivity and redox cycling. Although both of these mechanisms influence KAT-inhibitory activity, they are probably subsidiary mechanisms. However, these chemical events are the main causes of cellular toxicity. We therefore synthesized the molecule PTK1, which has a modification at the 3rd position and chemically differs from plumbagin. PTK1, having no thiol-reactive property, has fewer pleiotropic and toxic effects but still retains the ability to inhibit KAT. Stability conferred by a methyl substitution decreases the redox-cycling and thiol-reactive tendencies of PTK1 compared with plumbagin, thus improving the toxicity profile of PTK1. Therefore, investigations into the role of the chemical properties of 1,4-naphthoquinone analogs in cellular toxicity and the inhibition of acetyltransferase p300 have led to the synthesis of PTK1, a less toxic inhibitor. However, further modifications of this molecule are essential to improve its potency in the nanomolar range.

Acknowledgments—We thank Dr. T. Govindaraju and J. I. Mahesh (NMR Facility, New Chemistry Unit, JNCASR) for assistance with NMR spectral analysis. We thank Dr. D. Karthigeyan for help with the SERS experiment. We thank Dr. Mohammed Arif and Dr. Ruthrotha Selvi for valuable suggestions.

REFERENCES

1. Cole, P. A. (2008) Chemical probes for histone-modifying enzymes. *Nat. Chem. Biol.* **4,** 590–597
2. Selvi, B. R., Mohankrishna, D. V., Ostwal, Y. B., and Kundu, T. K. (2010) Small molecule modulators of histone acetylation and methylation. A disease perspective. *Biochim. Biophys. Acta* **1799,** 810–828
3. Mallavadhani, U. V., Panda, A. K., and Rao, Y. R. (1998) Pharmacology and chemotaxonomy of Diospyros. *Phytochemistry* **49,** 901–951
4. Ravindra, K. C., Selvi, B. R., Arif, M., Reddy, B. A., Thanuja, G. R., Agrawal, S., Pradhan, S. K., Nagashayana, N., Dasgupta, D., and Kundu, T. K. (2009) Inhibition of lysine acetyltransferase KAT3B/p300 activity by a naturally occurring hydroxynaphthoquinone, plumbagin. *J. Biol. Chem.* **284,** 24453–24464
5. Inbaraj, J. J., and Chignell, C. F. (2004) Cytotoxic action of juglone and plumbagin. A mechanistic study using HaCaT keratinocytes. *Chem. Res. Toxicol.* **17,** 55–62
6. Klaus, V., Hartmann, T., Gambini, J., Graf, P., Stahl, W., Hartwig, A., and Klotz, L. O. (2010) 1,4-Naphthoquinones as inducers of oxidative damage and stress signaling in HaCaT human keratinocytes. *Arch. Biochem. Biophys.* **496,** 93–100
7. Castro, F. A., Mariani, D., Panek, A. D., Eleutherio, E. C., and Pereira, M. D. (2008) Cytotoxicity mechanism of two naphthoquinones (menadione and plumbagin) in *Saccharomyces cerevisiae*. *PLoS One* **3,** e3999
8. Miller, M. G., Rodgers, A., and Cohen, G. M. (1986) Mechanisms of toxicity of naphthoquinones to isolated hepatocytes. *Biochem. Pharmacol.* **35,** 1177–1184
9. Lau, O. D., Kundu, T. K., Soccio, R. E., Ait-Si-Ali, S., Khalil, E. M., Vassilev, A., Wolffe, A. P., Nakatani, Y., Roeder, R. G., and Cole, P. A. (2000) HATs off. Selective synthetic inhibitors of the histone acetyltransferases p300 and PCAF. *Mol Cell.* **5,** 589–595
10. Liu, X., Wang, L., Zhao, K., Thompson, P. R., Hwang, Y., Marmorstein, R., and Cole, P. A. (2008) The structural basis of protein acetylation by the p300/CBP transcriptional coactivator. *Nature* **451,** 846–850
11. Bowers, E. M., Yan, G., Mukherjee, C., Orry, A., Wang, L., Holbert, M. A., Crump, N. T., Hazzalin, C. A., Liszczak, G., Yuan, H., Larocca, C., Saldanha, S. A., Abagyan, R., Sun, Y., Meyers, D. J., Marmorstein, R., Mahadevan, L. C., Alani, R. M., and Cole, P. A. (2010) Virtual ligand screening of the p300/CBP histone acetyltransferase. Identification of a selective small molecule inhibitor. *Chem. Biol.* **17,** 471–482
12. Balasubramanyam, K., Swaminathan, V., Ranganathan, A., and Kundu, T. K. (2003) Small molecule modulators of histone acetyltransferase p300. *J. Biol. Chem.* **278,** 19134–19140
13. Balasubramanyam, K., Altaf, M., Varier, R. A., Swaminathan, V., Ravindran, A., Sadhale, P. P., and Kundu, T. K. (2004) Polyisoprenylated benzophenone, garcinol, a natural histone acetyltransferase inhibitor, represses chromatin transcription and alters global gene expression. *J. Biol. Chem.* **279,** 33716–33726
14. Balasubramanyam, K., Varier, R. A., Altaf, M., Swaminathan, V., Siddappa, N. B., Ranga, U., and Kundu, T. K. (2004) Curcumin, a novel p300/CREB-binding protein-specific inhibitor of acetyltransferase, represses the acetylation of histone/nonhistone proteins and histone acetyltransferase-dependent chromatin transcription. *J. Biol. Chem.* **279,** 51163–561171
15. Mantelingu, K., Reddy, B. A., Swaminathan, V., Kishore, A. H., Siddappa, N. B., Kumar, G. V., Nagashankar, G., Natesh, N., Roy, S., Sadhale, P. P., Ranga, U., Narayana, C., and Kundu, T. K. (2007) Specific inhibition of p300-HAT alters global gene expression and represses HIV replication. *Chem. Biol.* **14,** 645–657
16. Arif, M., Vedamurthy, B. M., Choudhari, R., Ostwal, Y. B., Mantelingu, K., Kodaganur, G. S., and Kundu, T. K. (2010) Nitric oxide-mediated histone hyperacetylation in oral cancer. Target for a water-soluble HAT inhibitor, CTK7A. *Chem. Biol.* **17,** 903–913
17. Arif, M., Pradhan, S. K., Thanuja, G. R., Vedamurthy, B. M., Agrawal, S., Dasgupta, D., and Kundu, T. K. (2009) Mechanism of p300 specific histone acetyltransferase inhibition by small molecules. *J. Med. Chem.* **52,** 267–277
18. Pavan Kumar, G. V., and Narayana, C. (2007) Adapting a fluorescence microscope to perform surface enhanced Raman spectroscopy. *Curr. Sci.* **93,** 778–791
19. Arif, M., Karthigeyan, D., Siddhanta, S., Kumar, G. V., Narayana, C., and Kundu, T. K. (2013) Analysis of protein acetyltransferase structure-function relation by surface-enhanced Raman scattering (SERS). A tool to screen and characterize small molecule modulators. *Methods Mol. Biol.* **981,** 239–261
20. Lee, P. C., and Meisel, D. (1982) Adsorption and surface-enhanced Raman of dyes on silver and gold sols. *J. Phys. Chem.* **86,** 3391–3395
21. Frisch, M. J., Trucks, G. W., Schlegel, H. B., Scuseria, G. E., Robb, M. A., Cheeseman, J. R., Montgomery, J. A., Jr., Vreven, T., Kudin, K. N., Burant, J. C., Millam, J. M., Iyengar, S. S., Tomasi, J., Barone, V., Mennucci, B., Cossi M., Scalmani, G., Rega, N., Petersson, G. A., Nakatsuji, H., Hada, M., Ehara, M., Toyota, K., Fukuda, R., Hasegawa, J., Ishida, M., Nakajima, T., Honda, Y., Kitao, O., Nakai, H., Klene, M., Li, X., Knox, J. E., Hratchian, H. P., Cross, J. B., Adamo, C., Jaramillo, J., Gomperts, R., Stratmann, R. E., Yazyev, O., Austin, A. J., Cammi, R., Pomelli, C., Ochterski, J. W., Ayala, P. Y., Morokuma, K., Voth, G. A., Salvador, P., Dannenberg, J. J., Zakrzewski, V. G., Dapprich, S., Daniels, A. D., Strain, M. C., Farkas, O., Malick, D. K., Rabuck, A. D., Raghavachari, K., Foresman, J. B., Ortiz, J. V., Cui, Q., Baboul, A. G., Clifford, S., Cioslowski, J., Stefanov, B. B., Liu, G., Liashenko, A., Piskorz, P., Komaromi, I., Martin, R. L., Fox, D. J., Keith, T., Al-Laham, M. A., Peng, C. Y., Nanayakkara, A., Challacombe, M., Gill, P. M. W., Johnson, B., Chen, W., Wong, M. W., Gonzalez, C., and Pople, J. A. (2003) *GAUSSIAN 03*, Revision B.04, Gaussian Inc., Wallingford, CT
22. Morris, G. M., Huey, R., Lindstrom, W., Sanner, M. F., Belew, R. K., Goodsell, D. S., and Olson, A. J. (2009) AutoDock4 and AutoDockTools4. Automated docking with selective receptor flexibility. *J. Comput. Chem.* **30,** 2785–2791
23. Delano, W. L. (2004) *The PyMOL Molecular Graphics System*, DeLano Scientific LLC, San Carlos, CA
24. Ogihara, K., Yamashiro, R., Higa, M., and Yogi, S. (1997) Preparation of naphthoquinone derivatives from plumbagin and their ichthyotoxicity. *Chem. Pharm. Bull.* **45,** 437–445
25. Sandur S. K., Ichikawa, H., Sethi, G., Ahn, K. S., and Aggarwal, B. B. (2006) Plumbagin (5-hydroxy-2-methyl-1,4-naphthoquinone) suppresses NF-κB activation and NF-κB-regulated gene products through modulation of p65 and IκBα kinase activation, leading to potentiation of apoptosis induced by cytokine and chemotherapeutic agents. *J. Biol. Chem.* **281,** 17023–17033
26. Checker, R., Sharma, D., Sandur, S. K., Subrahmanyam, G., Krishnan, S., Poduval, T. B., and Sainis, K. B. (2010) Plumbagin inhibits proliferative and inflammatory responses of T cells independent of ROS generation but by modulating intracellular thiols. *J. Cell. Biochem.* **110,** 1082–1093
27. Powolny, A. A., and Singh, S. V. (2008) Plumbagin-induced apoptosis in human prostate cancer cells is associated with modulation of cellular redox status and generation of reactive oxygen species. *Pharm. Res.* **25,** 2171–2180
28. Kang, J., Chen, J., Shi, Y., Jia, J., and Zhang, Y. (2005) Curcumin-induced histone hypoacetylation. The role of reactive oxygen species. *Biochem. Pharmacol.* **69,** 1205–1213
29. Choudhury, M., Park, P. H., Jackson, D., and Shukla, S. D. (2010) Evidence for the role of oxidative stress in the acetylation of histone H3 by ethanol in rat hepatocytes. *Alcohol* **44,** 531–540
30. Kang, J., Zhang, Y., Chen, J., Chen, H., Lin, C., Wang, Q., and Ou, Y. (2003) Nickel-induced histone hypoacetylation. The role of reactive oxygen species. *Toxicol. Sci.* **74,** 279–286
31. Yu, M., Magalhães, M. L., Cook, P. F., Blanchard, J. S. (2006) Bisubstrate inhibition. Theory and application to *N*-acetyltransferases. *Biochemistry* **45,** 14788–14794
32. Arif, M., Kumar, G. V., Narayana, C., and Kundu, T. K. (2007) Autoacetylation induced specific structural changes in histone acetyltransferase domain of p300. Probed by surface enhanced Raman spectroscopy. *J. Phys. Chem. B* **111,** 11877–11879

33. Kumar, G. V., Selvi, R., Kishore, A. H., Kundu, T. K., and Narayana, C. (2008) Surface-enhanced Raman spectroscopic studies of coactivator-associated arginine methyltransferase 1. *J. Phys. Chem. B* **112,** 6703–6707
34. Mantelingu, K., Kishore, A. H., Balasubramanyam, K., Kumar, G. V., Altaf, M., Swamy, S. N., Selvi, R., Das, C., Narayana, C., Rangappa, K. S., and Kundu, T. K. (2007) Activation of p300 histone acetyltransferase by small molecules altering enzyme structure. Probed by surface-enhanced Raman spectroscopy. *J. Phys. Chem. B* **111,** 4527–4534
35. Siddhanta S., and Narayana, C. (2012) Surface enhanced Raman spectroscopy of proteins. Implications in drug designing. *Nanomater. Nanotechnol.* **2,** 1–13
36. Pavan Kumar, G. V., Ashok Reddy B. A., Arif, M., Kundu, T. K., and Narayana, C. (2006) Surface-enhanced Raman scattering studies of human transcriptional coactivator p300. *J. Phys. Chem. B* **110,** 16787–16792
37. Reipa, V., and Horvath, J. J. (1992) Surface-enhanced Raman study of benzylpenicillin. *Appl. Spectrosc.* **46,** 1009–1013
38. Srinivas, P., Gopinath, G., Banerji, A., Dinakar A., and Srinivas, G. (2004) Plumbagin induces reactive oxygen species, which mediate apoptosis in human cervical cancer cells. *Mol. Carcinog.* **40,** 201–211
39. Stimson, L., Rowlands, M. G., Newbatt, Y. M., Smith, N. F., Raynaud, F. I., Rogers, P., Bavetsias, V., Gorsuch, S., Jarman, M., Bannister, A., Kouzarides, T., McDonald, E., Workman, P., and Aherne, G. W. (2005) Isothiazolones as inhibitors of PCAF and p300 histone acetyltransferase activity. *Mol. Cancer Ther.* **4,** 1521–1532
40. Song, D., Gao, Y., Wang, R., Liu, D., Zhao, L., and Jing, Y. (2010) Down-regulation of c-FLIP, XIAP and Mcl-1 protein as well as depletion of reduced glutathione contribute to the apoptosis induction of glycyrrhetinic acid derivatives in leukemia cells. *Cancer Biol. Ther.* **9,** 96–108

Naphthoquinone-mediated Inhibition of Lysine Acetyltransferase KAT3B/p300, Basis for Non-toxic Inhibitor Synthesis

Mohankrishna Dalvoy Vasudevarao, Pushpak Mizar, Sujata Kumari, Somnath Mandal, Soumik Siddhanta, Mahadeva MM Swamy, Stephanie Kaypee, Ravindra C Kodihalli, Amrita Banerjee, Chandrabhas Naryana, Dipak Dasgupta and Tapas K. Kundu

J. Biol. Chem. 2014, 289:7702-7717.
doi: 10.1074/jbc.M113.486522 originally published online January 27, 2014
